Gravitational waves from the collapse and bounce of a stellar core in tensor-scalar gravity

Jérôme Novak[1] and José M$^{\underline{a}}$. Ibáñez

Departamento de Astronomía y Astrofísica, Universidad de Valencia, 46100 Burjassot, Spain

Received _____; accepted _____

[1]also at Département d'Astrophysique Relativiste et de Cosmologie (UMR 8629 C.N.R.S.), Observatoire de Paris, Section de Meudon, F-92195 Meudon Cedex, France

ABSTRACT

Tensor-scalar theory of gravity allows the generation of gravitational waves from astrophysical sources, like Supernovæ, even in the spherical case. That motivated us to study the collapse of a degenerate stellar core, within tensor-scalar gravity, leading to the formation of a neutron star through a bounce and the formation of a shock. We discuss in this paper the effects of the scalar field on the evolution of the system, as well as the appearance of strong non-perturbative effects of this scalar field (the so-called "spontaneous scalarization"). As a main result, we describe the resulting gravitational monopolar radiation (form and amplitude) and discuss the possibility of its detection by the gravitational detectors currently under construction, taking into account the existing constraints on the scalar field. From the numerical point of view it is worthy to point out that we have developed a combined code which uses pseudo-spectral methods, for the evolution of the scalar field, and High Resolution Shock-Capturing schemes, for the evolution of the hydrodynamical system. Although this code has been used to integrate the field equations of that theory of gravity, in the spherically symmetric case, a by-product of the present work is to gain experience for an ulterior extension to multidimensional problems in Numerical Relativity of such numerical strategy.

Subject headings: Gravitation – Gravitational waves – Methods: numerical – Supernova: general – Shock waves

1. Introduction

Tensor-scalar theories of gravitation (Damour & Esposito-Farèse (1992)) appear to be interesting alternatives to Einstein's General Relativity, which naturally arise from the low-energy limit of superstring theories (Damour & Polyakov (1994)). These theories also allow for a "graceful exit" from inflation (García-Bellido & Quirós (1990)). One of their main observational predictions is the emission of *monopolar* gravitational radiation, from quasi-spherical astrophysical objects. Previous works on collapses in tensor-scalar theories dealt with the gravitational collapse in tensor-scalar theories started with studying the Oppenheimer-Snyder (dust) collapse (Oppenheimer & Snyder(1939)) in the frame of the so-called "Jordan-Fierz-Brans-Dicke" theory, in which the coupling function (4) depends only on one parameter (Shibata et al. (1994) and Scheel et al. (1995)). The next work by Harada et al. (1997) considered a two-parameter coupling function (as in this work), but neglecting any non-perturbative effect from the scalar field. However, these non-perturbative effects can be very important in neutron stars, as have shown Damour & Esposito-Farèse (1993), making an analogy between this "spontaneous scalarization" of neutron stars and the spontaneous magnetization of ferromagnets (Damour & Esposito-Farèse (1996)). Novak (1998a) (paper I hereafter) dealt with the collapse of a neutron star to a black hole, including pressure and non-perturbative effects. We here study the emission of monopolar gravitational waves coming from the formation of a neutron star. The problem is quite different since, according to Hawking's "no-hair" theorem (Hawking (1972)), a black hole cannot possess any scalar charge, neutron stars appear to be the astrophysical object with the strongest possible scalar charge. Their formation (during a Supernova type Ib or type II event) is therefore a powerful and interesting source of gravitational radiation. The purpose of this paper is to present results from the numerical study of the collapse of a stellar core which forms a neutron star, within the framework of tensor-scalar theories and, namely, to explicit the resulting monopolar gravitational radiation.

Following paper I, we will consider only one scalar field φ and we will use two conformally related metrics $\tilde{g}_{\mu\nu} = a^2(\varphi) g^*_{\mu\nu}$, called the *Jordan-Fierz* (or physical) metric ($\tilde{g}_{\mu\nu}$) and the *Einstein* metric ($g^*_{\mu\nu}$). All the quantities with a tilde are related to the Jordan-Fierz metric, to which the matter is coupled. That means that all non-gravitational experiments measure this metric, although the field equations of the theory are better formulated in the Einstein one. The tensor-scalar field equations are

$$R^*_{\mu\nu} - \frac{1}{2} g^*_{\mu\nu} R^* = 2\partial_\mu\varphi\partial_\nu\varphi - g^*_{\mu\nu} g^{\rho\sigma}_* \partial_\rho\varphi\partial_\sigma\varphi + \frac{8\pi G_*}{c^4} T^*_{\mu\nu}, \tag{1}$$

for the tensor part, and

$$g_*^{\mu\nu}\nabla_\mu^*\nabla_\nu^*\varphi = -4\pi G_*\alpha(\varphi)T_* \tag{2}$$

for the scalar field.

The Einstein-frame stress-energy tensor $T_*^{\mu\nu}$ is related to the physical one by the arbitrary coupling function $a(\varphi)$

$$T_{*\nu}^{\mu} = a^4(\varphi)\tilde{T}_\nu^\mu. \tag{3}$$

The function $\alpha(\varphi)$ is the logarithmic derivative of $a(\varphi)$ and represents the field-dependent coupling strength between matter and the scalar field. We will assume it is well represented by a linear function (see Novak (1998b) for more details):

$$\alpha(\varphi) = \alpha_0 + \beta_0 \times (\varphi - \varphi_0). \tag{4}$$

The arbitrary function $a(\varphi)$ is determined by the two parameters (α_0, β_0) (φ_0, the scalar field at spatial infinity, is redundant with α_0). We will also consider the collapse to be spherically symmetric, since we are concerned with monopolar radiation, which should be dominant over higher terms in such events.

The paper is organized as follows: Section 2 presents the gauge choice, the tensor-scalar equations derived in this gauge (Sec. 2.1) and the numerical method used for integrating them (Sec. 2.2), as well as the performed tests (Sec. 2.3). Section 3 is dedicated to the simulations which were done; namely, the physical models used (3.1), results of the simulations (3.2) and a discussion on the resulting gravitational waves and their interaction with the detectors (3.3). Finally, Section 4 summarizes the results and gives some concluding remarks.

2. Equations and numerical issues

As in Paper I, we have chosen the *Radial Gauge* and *Polar Slicing* (Schwarzschild-like coordinates), the metric being diagonal:

$$ds^2 = -N^2(r,t)dt^2 + A^2(r,t)dr^2 + r^2(d\theta^2 + \sin^2\theta d\phi^2), \tag{5}$$

where $N(r,t)$ is called the *lapse function*. The metric $g_{\mu\nu}^*$ will often be described by the three auxiliary functions $\nu(r,t)$, $m(r,t)$ and $\zeta(r,t)$ defined by

$$N(r,t) = \exp(\nu(r,t)),$$
$$A(r,t) = \left(1 - \frac{2m(r,t)}{r}\right)^{-1/2},$$

$$\zeta(r,t) = \ln\left(\frac{N}{A}\right).$$

All coordinates are expressed in the Einstein frame, and asterisks are omitted. However, "physical" quantities will often be written with a tilde, that is in the Jordan-Fierz frame. The matter is supposed to be modeled by a perfect fluid:

$$\tilde{T}_{\mu\nu} = (\tilde{e}+\tilde{p})\tilde{u}_\mu\tilde{u}_\nu + \tilde{p}\tilde{g}_{\mu\nu}, \tag{6}$$

where $\tilde{u}_\mu$ is the 4-velocity of the fluid, $\tilde{e}$ is the total energy density (including rest mass) in the fluid frame and $\tilde{p}$ is the pressure.

2.1. Equations in RGPS gauge

As far as the hydrodynamics are concerned, we will use a set of *primitive variables* $\{\tilde{n}_B, \tilde{e}, U\}$, which are respectively the baryonic and the total energy densities in the fluid frame, and the fluid radial velocity:

$$U = \frac{A}{N}\frac{\tilde{u}^r}{\tilde{u}^0};$$

$\Gamma = (1-U^2)^{-1/2}$ being the Lorentz factor of the fluid. We also use the variable:

$$\tilde{E} = -\tilde{T}^0_0 = \Gamma^2(\tilde{e}+\tilde{p}) - \tilde{p},$$

and three "scalar-field" variables:

$$\eta = \frac{1}{A}\frac{\partial\varphi}{\partial r},\ \psi = \frac{1}{N}\frac{\partial\varphi}{\partial t},\ \Xi = \eta^2+\psi^2.$$

Considering the conservation of the stress-energy tensor and of the baryonic number (Cf. Paper I), one can write the hydrodynamical equations for evolution in a hyperbolic form[2]:

$$\frac{\partial\vec{u}}{\partial t} + \frac{1}{r^2}\frac{\partial}{\partial r}\left[r^2\frac{N}{A}\vec{f}(\vec{u})\right] = \vec{s}(\vec{u}), \tag{7}$$

where $\vec{u} = \{D^*, \mu^*, \tau^*\}$ is the *vector of unknowns* (evolved quantities), defined as

$$\begin{aligned} D^* &= a^4(\varphi)A\Gamma\tilde{n}_B, \\ \mu^* &= a^4(\varphi)\left(\tilde{E}+\tilde{p}\right)U, \\ \tau^* &= a^4(\varphi)\tilde{E} - D^*. \end{aligned} \tag{8}$$

[2]the equation for the density is not strictly in that form, see hereafter, at the end of the section

The associated vectors of fluxes $\vec{f}(\vec{u})$ and sources $\vec{s}(\vec{u})$ being (we define $q_\pi = 4\pi G_*/c^4$):

$$\begin{aligned} f_{D^*} &= UD^* \\ f_{\mu^*} &= \mu^* U + a^4(\varphi)\tilde{p} \\ f_{\tau^*} &= \mu^* - UD^*. \end{aligned} \tag{9}$$

and

$$\begin{aligned} s_{D^*} &= \alpha(\varphi)a(\varphi)D^*\frac{\partial\varphi}{\partial t} \\ s_{\mu^*} &= NA\left\{(\mu^*U - \tau^* - D^*)\left(2q_\pi r p^* + \frac{G_* m}{r^2c^2} + \frac{\alpha(\varphi)\eta}{A}\right) + p^*\frac{G_* m}{r^2c^2} + \frac{2p^*}{A^2 r}\right. \\ &\quad \left. + \frac{3\alpha(\varphi)p^*\eta}{A} - 2r\mu^*\eta\psi - \frac{r}{2}\Xi\left(\tau^* + D^* + p^*\right)\left(1+U^2\right)\right\} \\ s_{\tau^*} &= \left(\tau^* + D^* + p^*\right)NAr\left\{(1+U^2)\psi\eta + U\Xi\right\} - s_{D^*}. \end{aligned} \tag{10}$$

With this formulation, we easily recover the set of hydrodynamical equations in General Relativity, in the limit ($\varphi \to \varphi_0,\ a(\varphi) \to 1$), as described in Romero et al. (1996). Here, however, the evolution equation for the relativistic density (D^*) is not strictly in the form (7), but writes:

$$\frac{\partial D^*}{\partial t} + \frac{a(\varphi)}{r^2}\frac{\partial}{\partial r}\left[r^2\frac{N}{A}f_D^*\right] = s_{D^*}, \tag{11}$$

The system of equations is completed by an equation of state $\tilde{p} = \tilde{p}(\tilde{n}_B, \tilde{e})$, which will be detailed in Sec. 3.1, and the field equations for the metric and the scalar field:

$$\frac{\partial m}{\partial r} = \frac{c^2}{G_*}r^2\left(\Xi + q_\pi(\tau^* + D^*)\right), \tag{12}$$

$$\frac{\partial \nu}{\partial r} = \frac{q_\pi A^2}{2}\left(\frac{mc^2}{4\pi r^2} + r(\Xi + f_{\mu^*})\right), \tag{13}$$

$$\frac{\partial^2\varphi}{\partial t^2} = e^{2\zeta}\left(\Delta\varphi + \frac{\partial\zeta}{\partial r}\frac{\partial\varphi}{\partial r}\right) + \frac{\partial\zeta}{\partial t}\frac{\partial\varphi}{\partial t} - \frac{q_\pi}{2}\alpha(\varphi)T_*. \tag{14}$$

For more details on the derivations of this system, see Gourgoulhon (1991), Paper I and Romero et al. (1996). The key point is the choice of the conserved quantities (8) which, in tensor-scalar theories, keeps the system in a strictly hyperbolic form (7).

2.2. Numerical integration

As it will be discussed in Sec. 3.1, shocks are expected to appear in the simulations. It is then clear that the numerical integration must be able to handle such discontinuities. The code used in Paper I is

based on pseudo-spectral techniques and so, is not well adapted for this kind of problem. However, in one dimension Bonazzola & Marck (1991) have adapted the spectral methods to the case where a shock was present. This technique will not be used here, since we are interested in generalizing (in a future work) techniques developed here to two- and three-dimensional calculations. All the details of the numerical techniques will not be described here, one can refer to Romero et al. (1996) and Martí (1997) for the Godunov-type (High-Resolution Shock-Capturing, hereafter HRSC) methods and to Paper I and references therein for the spectral methods.

The idea is then to use two different numerical grids to describe the same physical space (using the same coordinates). These two grids allow for two different numerical techniques for solving the (7) – (14), governing the evolution of the matter and fields. The HRSC methods, on a grid with a rather large number of points (typically a few hundreds), are used to solve the hydrodynamical hyperbolic system (7), for they are the most efficient in handling discontinuous quantities, such as density or velocity after the bounce. Spectral methods are used to describe gravitational fields ($g^*_{\mu\nu}$ and φ), which are smooth, as well as their first derivative. In this work, for the equations of the Sec. 2.1 only the wave equation (14) has been integrated by those means, the two constraint equations, (12) and (13), giving the metric are very simple in the RGPS gauge and were integrated by usual finite-difference method.

Last but not least, the numerical information of the various fields has to be passed from one grid to the other paying special attention to minimize the numerical noise, not to destabilize the integration schemes. Getting from the spectral grid (spectral representation of functions as a truncated series of Chebyshev polynomials) to the HRSC one shows no difficulties, since a function, represented by its Chebyshev coefficients, can be evaluated at any point of its definition interval with a high precision as a (truncated) series and using the properties of Chebyshev polynomials (see e.g. Bonazzola et al.(1997)). Nevertheless, the interpolation in the other way (from HRSC grid to the spectral one) has to be "smooth" enough in order not to bring high frequency terms. The method used here meets these requirements, since functions are interpolated in the smoothest way, introducing no spurious information (Bonazzola (1998)). The interpolated points are such that the resulting amplitude of the function f, calculated as

$$\int_{\text{interval}} \left(\frac{d^2 f}{dx^2} \right)^2 ,$$

is minimized. This ensures that the Chebyshev coefficients of the interpolated function decrease fast enough and the overall series converges.

The resulting code (RSSM in the next,RS stands for Riemann Solvers and SM for Spectral Methods) is

then just the combination of an HRSC module, integrating in time the hydrodynamical variables $\{\tilde{n}_B, \tilde{e}, U\}$ and resolving the constraint equations giving m and ν. The source term of the wave equation (14) is then evaluated on the HRSC grid and interpolated to the spectral grid. Then, the wave equation is integrated to get the scalar field, which is computed, on the HRSC grid from its Chebyshev coefficients. The typical number of points used for the HRSC grid is between 300 and 500; for the spectral grid it is between 65 and 129.

2.3. Tests of the code

The *HRSC part* of the code comes directly from the code presented in Romero et al. (1996), in which numerous tests are shown. The *spectral part*, solving the wave equation, has been presented and tested in Paper I. The *interpolation procedure* has been tested on various analytical functions. The combined code, as a whole, has been checked by setting the scalar field to its asymptotic value φ_0 (as well as the coupling function $\alpha(\varphi)$ (4)), which gave us the general-relativistic results. On the other hand, putting the pressure to zero enabled us to retrieve the *dust collapse* of previous studies (Shibata et al. (1994), Scheel et al. (1995) and Harada et al. (1997)).

Finally, we tried to follow the *collapse of a neutron star to a black hole*, to compare with previous results from Paper I, but with this combined code. The initial model taken is a neutron star with a polytropic equation of state (see hereafter eq. 15). Since HRSC methods do not achieve the same precision as spectral ones, the collapse has to be triggered in a artificial way: decreasing the adiabatic index γ or the K coefficient of the equation of state:

$$\tilde{e}(\tilde{n}_B) = \tilde{n}_B\tilde{m}_B + K\frac{\tilde{n}_0\tilde{m}_B}{\gamma-1}\left(\frac{\tilde{n_B}}{\tilde{n}_0}\right)^\gamma$$
$$\tilde{p} = K\tilde{n}_0\tilde{m}_B\left(\frac{\tilde{n_B}}{\tilde{n}_0}\right)^\gamma. \qquad (15)$$

$\tilde{m}_B$ is the mass of one baryon ($= 1.66 \times 10^{-27}$kg) and $\tilde{n}_0 = 0.1\text{fm}^{-3}$. The resulting scalar waveform (see Sec. 3.2), computed by both codes separately is displayed on Fig. 1. The discrepancy is quite important at the beginning of the collapse, where the instability has to develop and the HRSC methods are less accurate. In addition, the boundary conditions imposed on the hydrodynamical system are not rigorously the same: as mentioned in Paper I, the spectral code uses a comoving grid, and there is only one boundary condition to impose which is chosen to be $\frac{1}{r^2}\frac{\partial}{\partial r}r^2U\big|_{r=R_{star}} = 0$; the HRSC methods use an *Eulerian* grid and impose three boundary conditions, chosen to be $f_{D^*} = f_{\mu^*} = f_{\tau^*} = 0$ at the boundary of the grid. This can

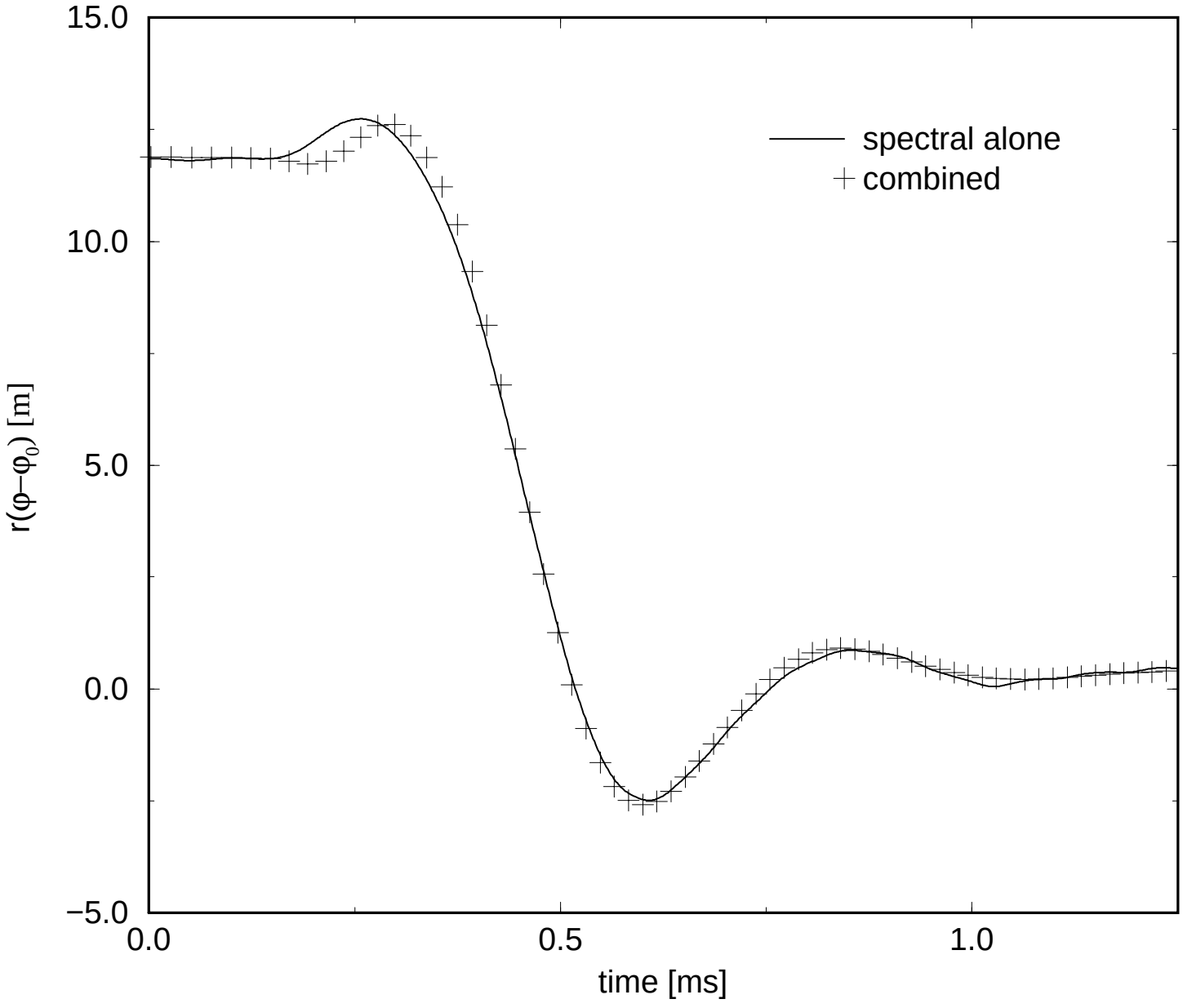

Fig. 1.— Comparison between the pure spectral code and the combined (HRSC and spectral) for the collapse of a neutron star, of baryonic mass 2.2 $M_\odot$ and with $\alpha_0 = 2.5 \times 10^{-3}$, $\beta_0 = -4$. Time origin is arbitrary.

influence the beginning of the collapse, but after that, the evolution is fast enough and such discrepancies disappear.

3. Simulations

As it has been mentioned above, the physical scenario we are considering is that of the formation of a neutron star.

3.1. The model

One can think of two ways to come to a neutron star: the collapse of the iron core of a massive star at the end of its evolution, i.e. the standard mechanism of type II supernova (Shapiro & Teukolsy (1983)), or the accretion induced collapse of a white dwarf which, under some conditions, can be non-explosive (Canal (1990)). In any case, the degeneracy pressure of the electrons can no longer support the gravity of the core and the collapse is unavoidable. When the central density becomes comparable to that of nuclear matter, the strong interactions between nucleons stiffen the equation of state. A strong shock is then generated according to the well known model for *prompt* mechanism of supernova (see Müller (1997) for details).

Since we are interested in the emission of monopolar gravitational radiation in the framework of a tensor-scalar theory of gravity, we have simplified the micro-physics concerning the equation of state (see below) and the neutrino transport (which has been neglected). The equation of state we consider is that of a perfect fluid for which the adiabatic index

$$\gamma = \left.\frac{\mathrm{d}\ln\tilde{p}}{\mathrm{d}\ln\tilde{n}_B}\right|_{\mathrm{adiab.}} \tag{16}$$

is not constant throughout the evolution of the collapsing star, but is *a priori* dependent on the density, temperature and chemical composition of matter. During the collapse, the adiabatic index is supposed to be lower than 4/3, but when the strong interactions between nucleons become dominant over other pressures, the adiabatic index grows rapidly above 4/3 and even 2. We can also consider that all the matter in the core follows roughly the same trajectory in the density-temperature space (see Arnett (1977) and Van Riper (1978)). In a first approximation, the adiabatic index thus depends only on the density:

$$\gamma(\tilde{n}_B) = \gamma_{\min} + S\left(\log_{10}(\tilde{\rho}) - \log_{10}(\rho_{\mathrm{bounce}})\right) \tag{17}$$

where $\tilde{\rho} = \tilde{m}_B\tilde{n}_B$, and ($\rho_{\mathrm{bounce}}$, S) are two parameters of the equation of state. There are other simplified

versions of the equation of state, which try to minimize the complex physics involved (see e.g. Müller (1997)). In this work we use (17)and we have taken $\gamma_{\rm min} = 1.33$ in all our runs. Table 1 summarizes the different parameter used for the models studied in this work. Models A, C and E use "standard" values for the equation of state parameters, whereas models B and D will produce a "stiffer" bounce and allow to explore higher central densities. This second type of model, even if it seems less realistic, allows for more relativistic regimes (the resulting neutron star being more compact), with stronger shocks. The initial state is the same as in Romero et al. (1996): a white dwarf of $1.39 M_{\odot}$, which is the maximal mass for such objects, as derived in Ibañez (1984). Models A and B are the same as in Romero et al. (1996), and will be used as general-relativistic calibrations, to compare with tensor-scalar results.

3.2. Results

We briefly show the results of general-relativistic simulations (models A and B of Tab. 1). We retrieve the results of Romero et al. (1996), but with the combined code, which is evolving a constant (equal to φ_0) scalar field (with a null coupling function (4)). Figs. 2 and 5 gives the velocity profiles for both simulations: both show the characteristic "V" shape during the infall epoch (labels 1,2 and 3 for Fig. 2, and 1 and 2 for Fig. 5). When the density near the center becomes larger than $\tilde{\rho}_{bounce}$ (see Figs. 3 and 6), the infall is stopped and the matter coming from outer layers is stopped and a shock appears propagating outward (labels 4 to 9 of Fig. 2 and 3 to 9 of Fig. 5). Central density reaches its maximum when the bounce happens (Figs. 3 and 6) and then settles to an equilibrium value. The evolution of the lapse is similar (see Figs. 4 and 7), and one can see that the final state of model B is more compact than A, even if the value of the central density is not compatible with these which are usually admitted for neutron stars (see e.g. Salgado

model	A	B	C	D	E
α_0	0.	0.	-0.01	-0.01	-1×10^{-3}
β_0	0	0	-4	-4	-7
$\tilde{\rho}_{\rm bounce}$ $[\rho_{\rm nuc}]$	1.5	15	1.5	15	1.5
S	1	5	1	5	1

Table 1: Parameters of the equation of state and of the coupling function (4), for the runs presented in this work. We took 1 $\rho_{\rm nuc} = 1.66 \times 10^{17}$ kg $\cdot$ m^{-3}.

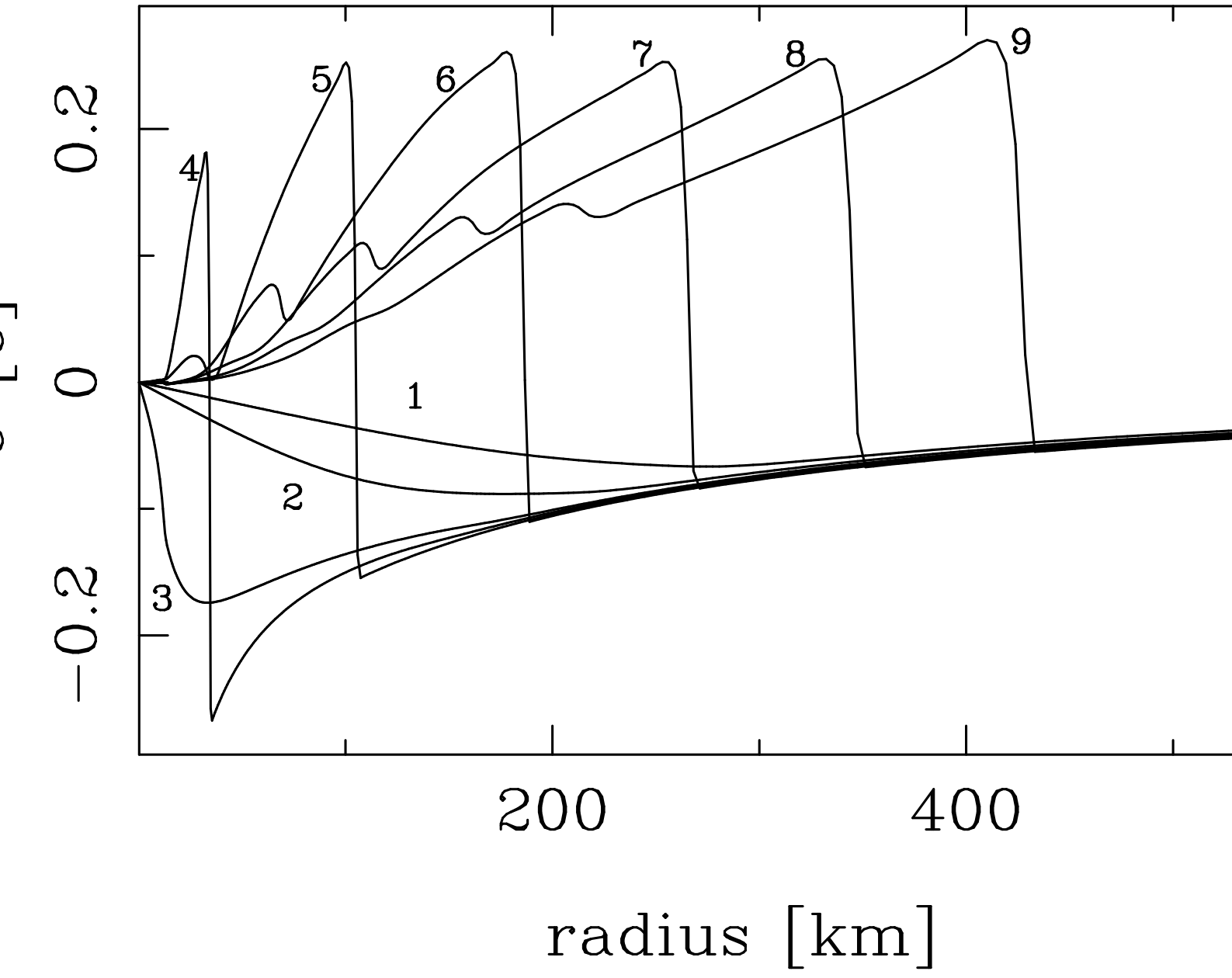

Fig. 2.— Snapshots of the fluid velocity U, as a function of the radius, at different moments of the collapse and bounce, for the model A of Tab. 1. Labels indicate time evolution (1:t=71.2 ms; 2: 76.3 ms; 3: 80.0 ms; 4:81.3 ms; 5: 82.4 ms; 6: 83.5 ms; 7: 84.7 ms; 8: 85.8 ms; 9: 86.9 ms).

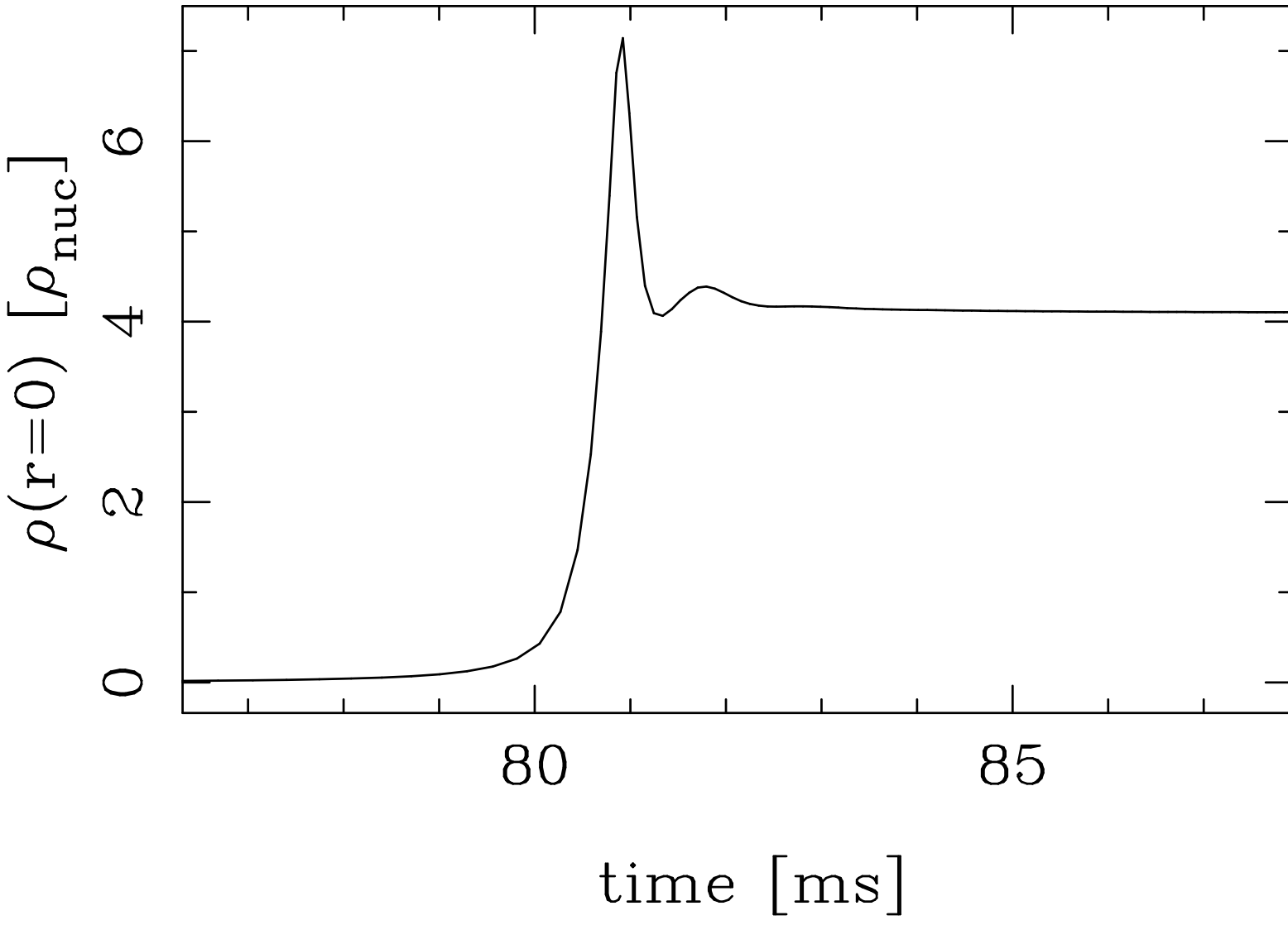

Fig. 3.— Evolution in time of the central density of the star, for the model A of Tab. 1

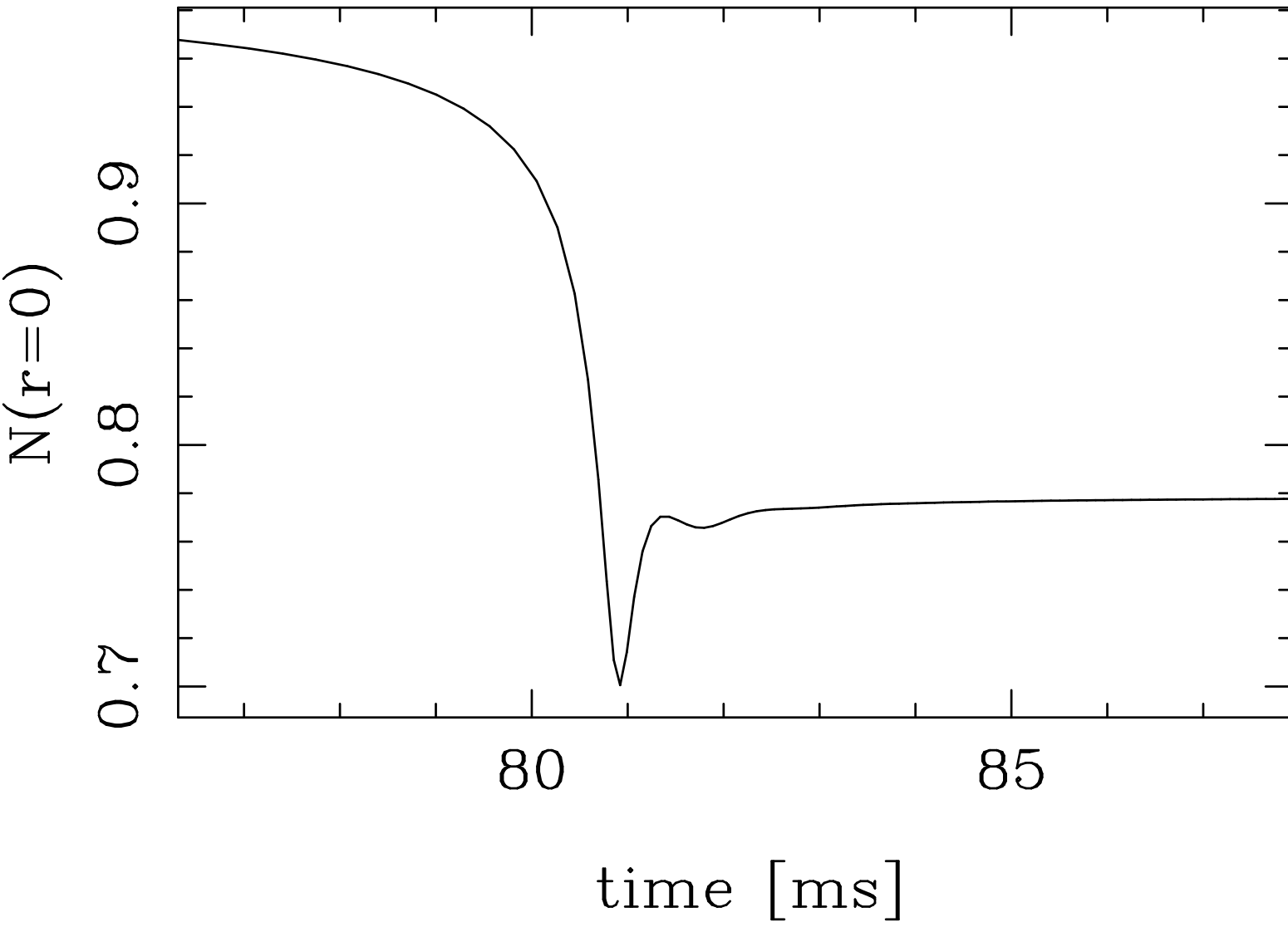

Fig. 4.— Evolution in time of the lapse at the center of the star, for the model A of Tab. 1

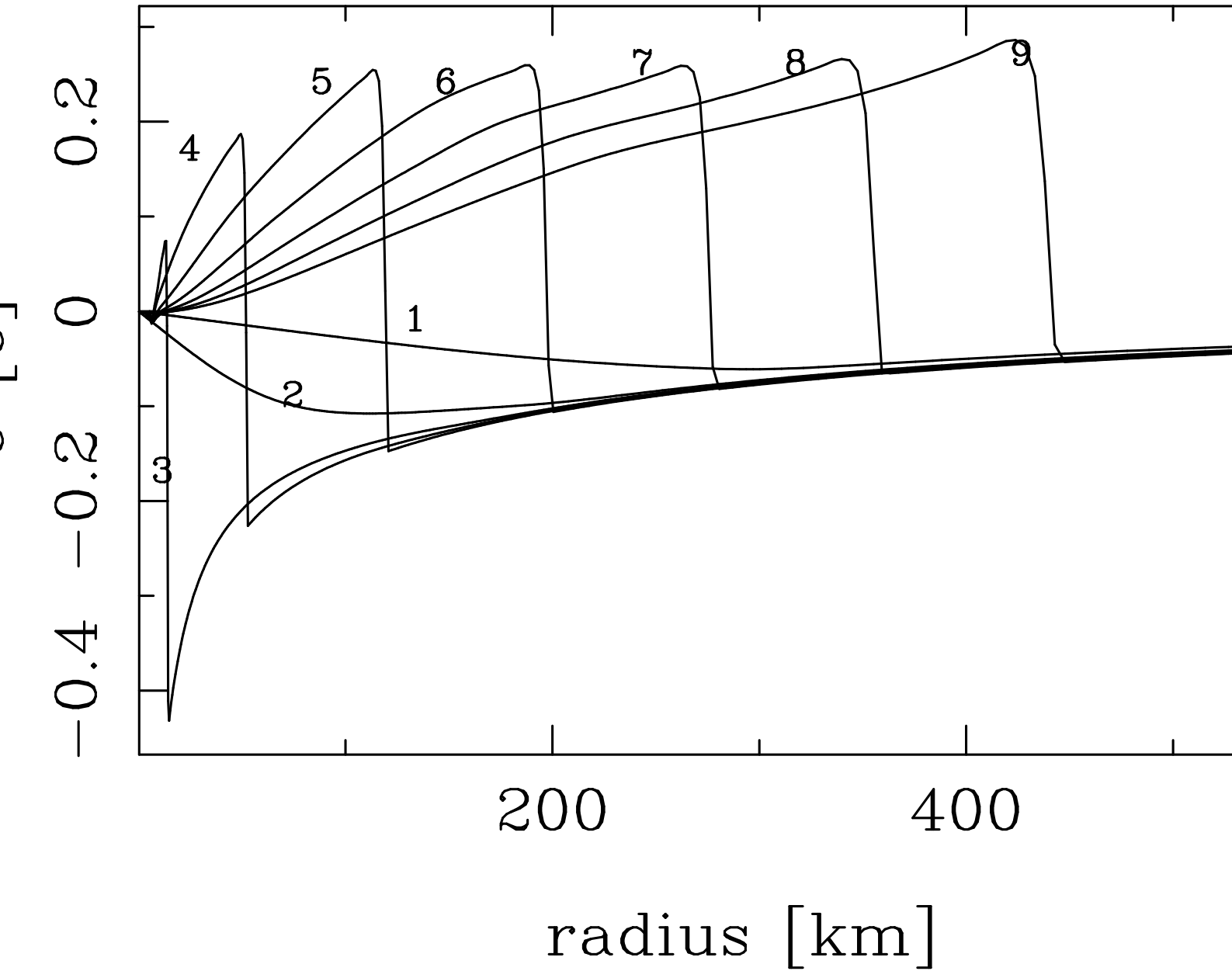

Fig. 5.— Snapshots of the fluid velocity U, as a function of the radius, at different moments of the collapse and bounce, for the model B of Tab. 1. Labels indicate time evolution(1:t=73.8 ms; 2: 79.6 ms; 3: 81.1 ms; 4:81.8 ms; 5: 82.6 ms; 6: 83.4 ms; 7: 84.2 ms; 8: 85.1 ms; 9: 85.9 ms).

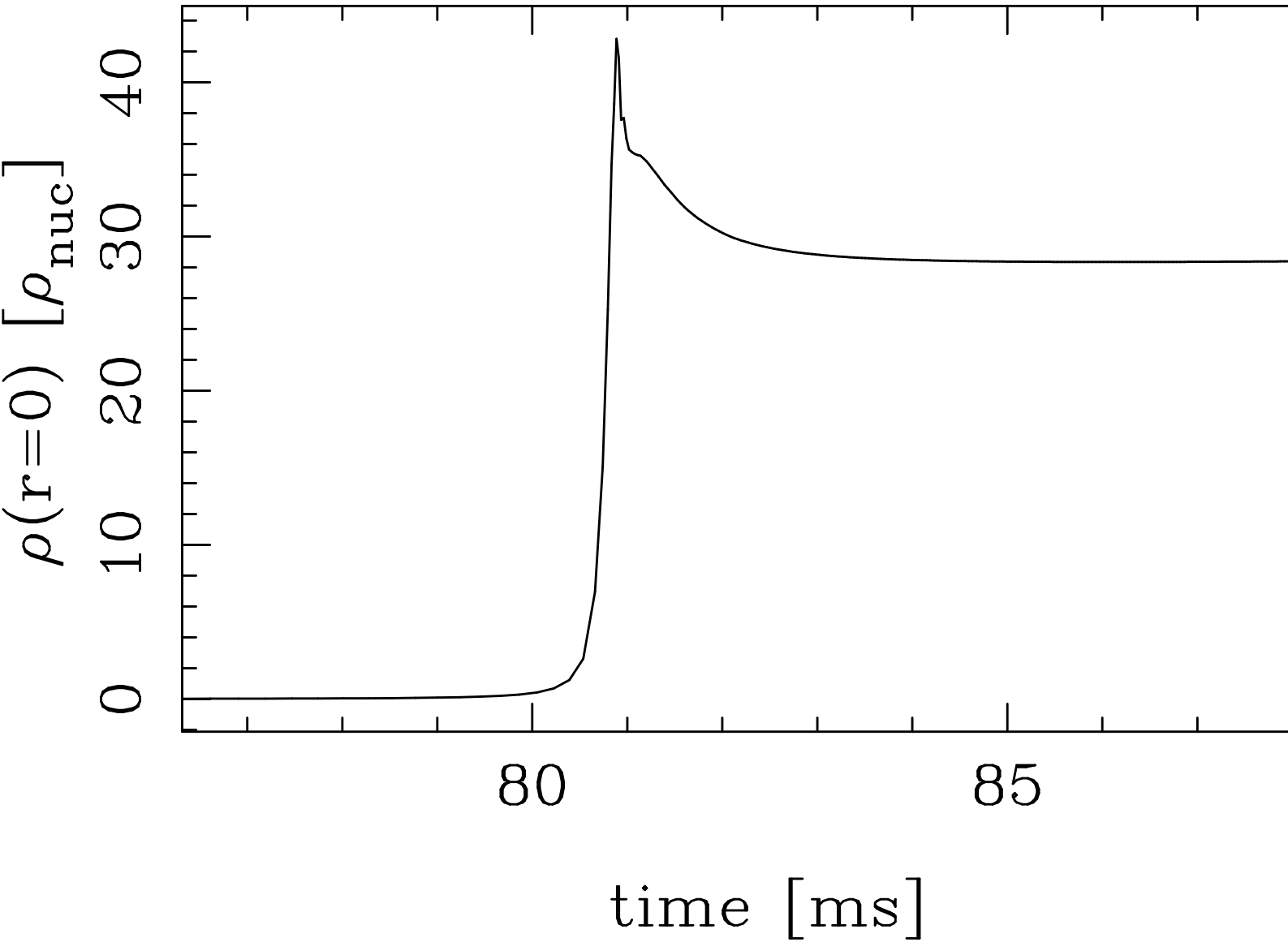

Fig. 6.— Evolution in time of the central density of the star, for the model B of Tab. 1

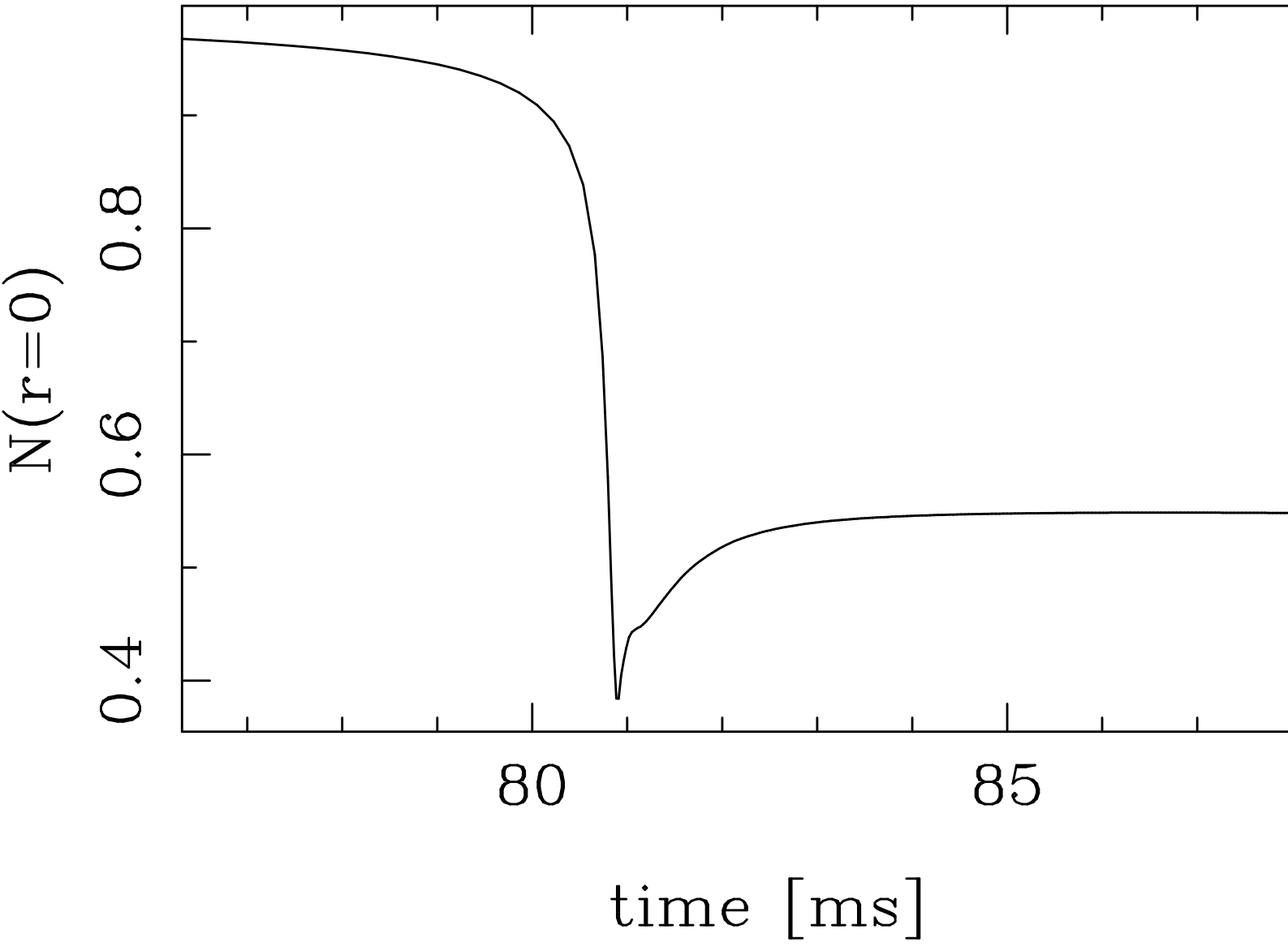

Fig. 7.— Evolution in time of the lapse at the center of the star, for the model B of Tab. 1

et al. (1994)).

We now turn to the tensor-scalar theory with the numerical evolution of models C, D and E of Tab. 1. Cases C and D have coupling function parameters that do not allow for the so-called "spontaneous scalarization" (see Novak (1998b)), for β_0 is not negative enough. Table 2 summarizes some results of the simulations. The most important difference between these runs and the general relativistic ones comes from the gravitational radiation emitted during the collapse (see Fig. 11 and 12), which will be discussed hereafter. These two figures also show the evolution of the scalar field during the collapse, the differences between both being related to the fact that the case D is more relativistic than C. The resulting neutron star being more compact for D, the scalar field reaches higher values and its influence on the final state begins to be noticeable. In both cases, in the beginning (until $t = 82$ ms), the scalar field only "follows" the matter, producing the spike at $t = 82$ ms in both figures. Then, in the C case, the scalar field varies as the star's central density. Nevertheless, in the D case, the scalar field has not reached its equilibrium value yet, so it continues to grow. However, the differences between general-relativistic and weak scalar field runs (A and C or B and D) are very small, the only one noticeable is the difference in the kinetic energy of the matter reaching escape velocity, between runs B and D. This can be seen as if the scalar field deepens the gravitational potential (which will be confirmed by the study of the case E), by locally increasing the gravitational coupling function (see Damour & Esposito-Farèse (1992)). The figures showing the evolution of central density, of the lapse and snapshots of velocity distribution are not displayed, for they are indistinguishable from those of General Relativity.

The case E has parameters of the coupling function (4) allowing *a priori* for a spontaneous scalarization of the neutron star. The results shown in Tab. 2 suggest that has indeed happened: scalar charge and resulting gravitational radiation are (at least) one order of magnitude higher than for the C case. The figure 8 shows the fluid velocity profile after the bounce, which exhibits a series of oscillations behind the shock. These oscillations are no numerical noise since a change in the number of points in the grids gives the same result and, most of all, the frequency of these oscillations corresponds to that of a neutron star undergoing a transition to a "spontaneous scalarization" state (Novak (1998b)). It is particularly interesting to compare Fig. 4 in this reference and Fig. 9 of this work. Let us recall that the numerical code used in Novak (1998b) is using only *spectral methods* and has been extensively tested; moreover, the particular simulation of transition to "spontaneous scalarization" has been verified by comparing the final data of the evolution (which represent a stable equilibrium configuration) with the results given by a static code. As it can be seen of Figs. 9 and 10, the whole proto-neutron star oscillates, looses energy through monopolar

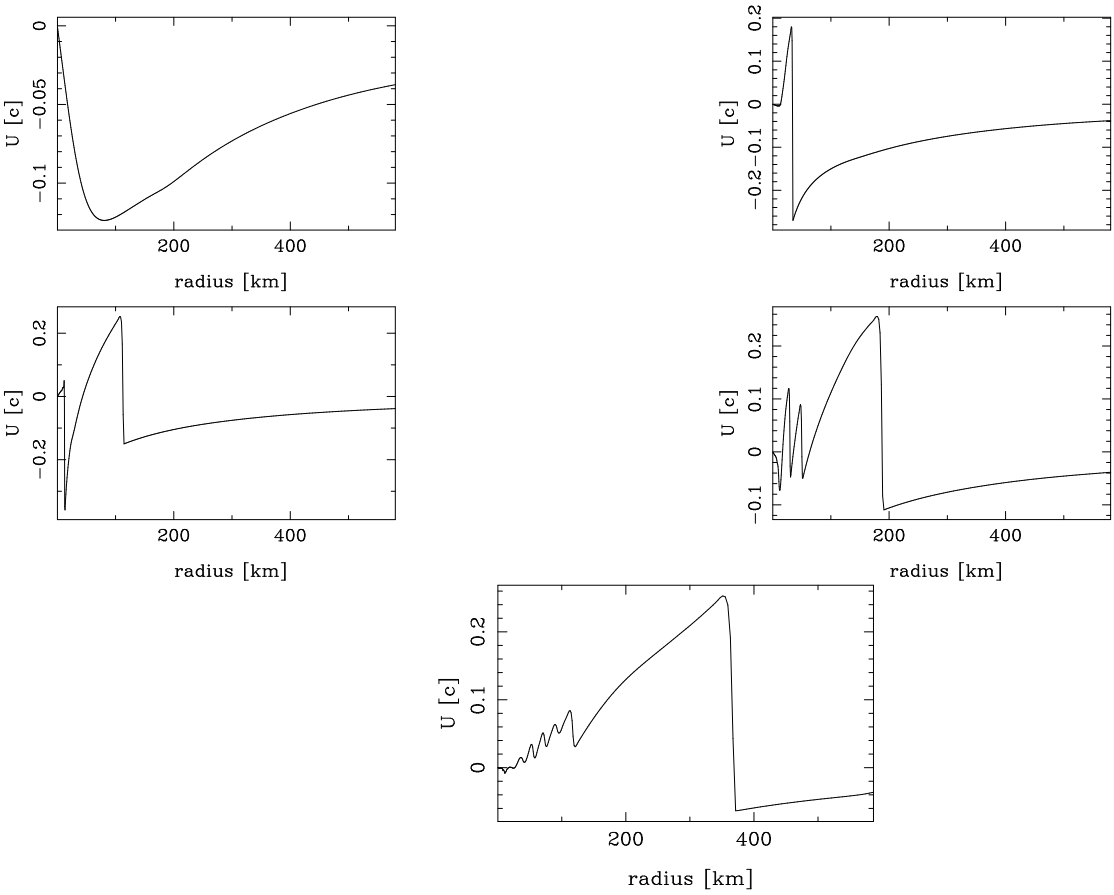

Fig. 8.— Profiles of the velocity, as a function of the radius, for the model E of Tab. 1, before and after the bounce(from left to right and top to bottom). Times are the following (t=80.0 ms, 81.3 ms, 82.3 ms, 83.0 ms and 84.6 ms). The oscillations behind the shock are due to the oscillation of the new-born neutron star.

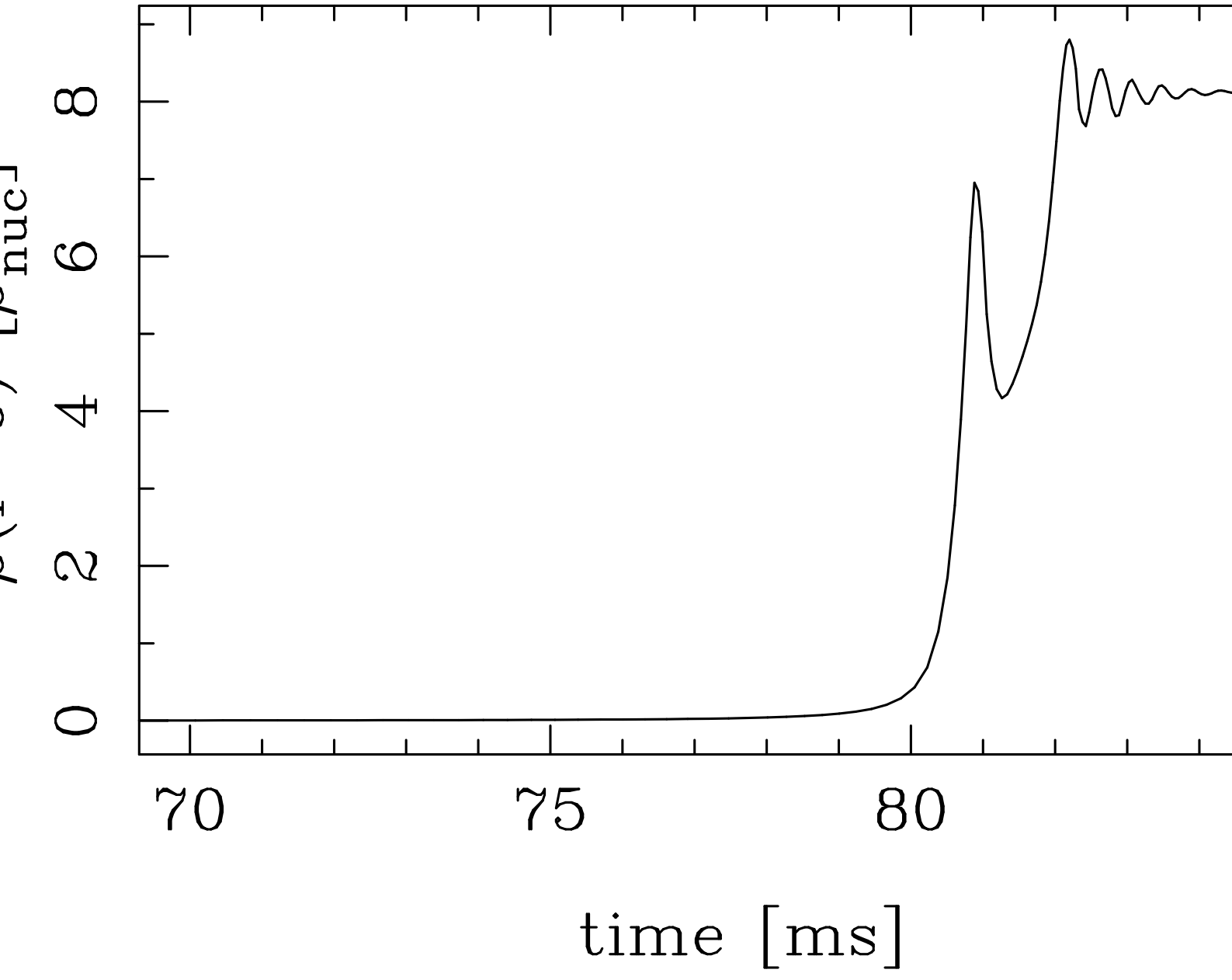

Fig. 9.— Evolution in time of the density at the center of the star, for the model E of Tab. 1

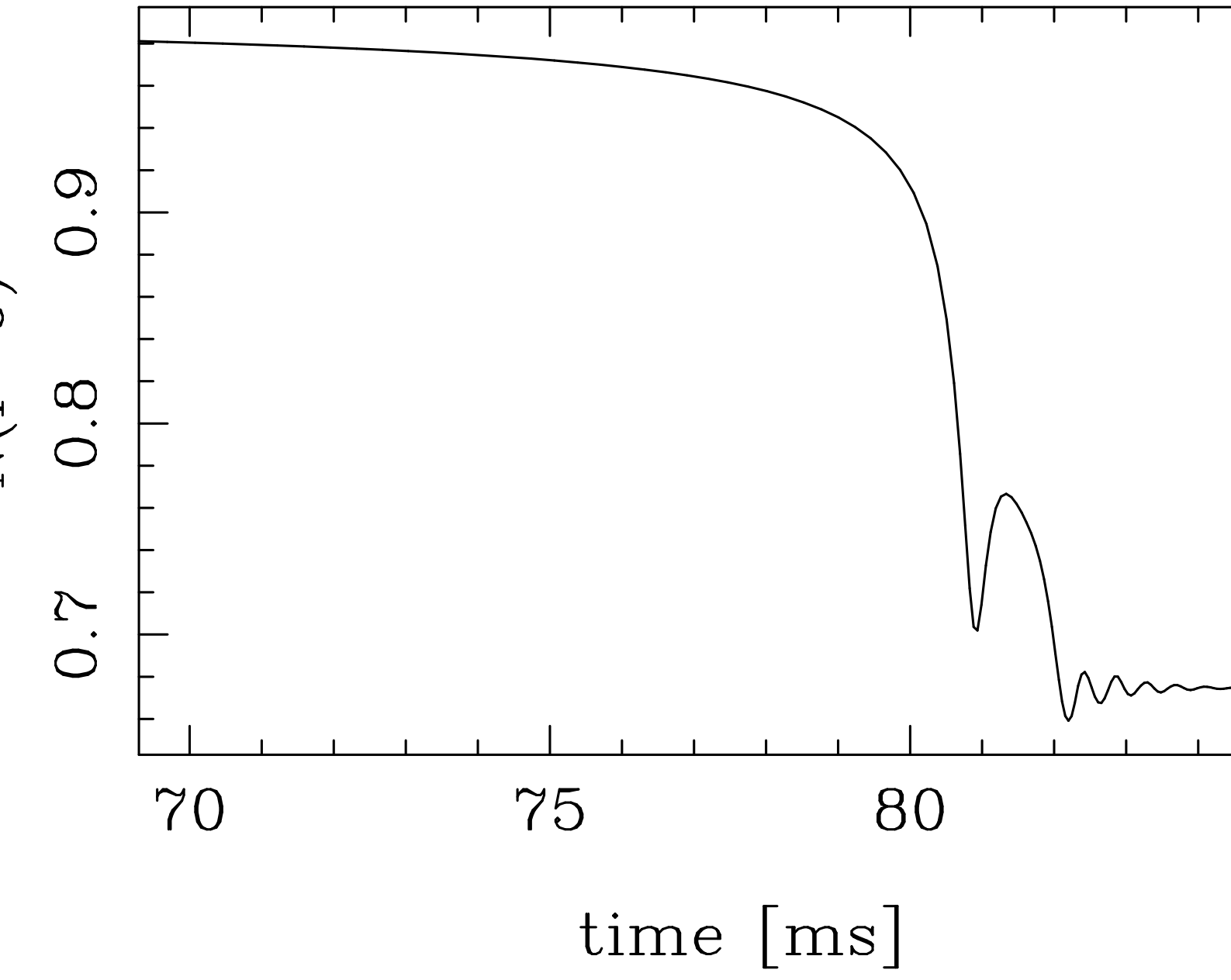

Fig. 10.— Evolution in time of the lapse at the center of the star, for the model E of Tab. 1

model	A	B	C	D	E
M_g $[M_\odot]$	1.2	1.1	1.2	1.1	1.2
R_{-3} [km]	31	15	31	15	21
ω $[M_\odot]$	0	0	$2.3 \cdot 10^{-2}$	$7 \cdot 10^{-2}$	0.52
$E_{\rm kin}$ $[10^{-3} M_\odot c^2]$	2.6	4.1	2.6	3.8	1.9
$\rho_{\rm max}$ $[\rho_{\rm nuc}]$	7	43	7	43	8.1
$N_{\rm min}$	0.71	0.38	0.71	0.38	0.64
$r\delta\varphi$ [m]	0	0	27	100	800
$E_{\rm rad}$ $[10^{-3} M_\odot c^2]$	0	0	$1.3 \cdot 10^{-3}$	$3.2 \cdot 10^{-2}$	0.8

Table 2: Various quantities measured during the numerical evolution of models described in Tab. 1. M_g is the gravitational mass of the resulting neutron star, ω its scalar charge (defined as the monopolar part of the static scalar field, see Damour & Esposito-Farèse (1993) for more details) and R_{-3} is such that $\tilde{\rho}(R_{-3}) = 10^{-3}\tilde{\rho}(r = 0)$. $E_{\rm kin}$ and $E_{\rm rad}$ are the kinetic energy of the matter reaching the escape velocity when the shock comes to $r = 600$ km, and the radiated gravitational energy as a monopolar wave. $\rho_{\rm max}$ is the maximal value reached by the central density $N_{\rm min}$ the minimal value of the lapse and $r\delta\varphi$ is related to the amplitude of the scalar gravitational wave by (19).

radiation and settles down to a strong scalar field state. We also have the confirmation that the scalar field deepens the gravitational potential well: comparing the run E to A and C, one sees that the neutron star is more compact and that the ejected matter has less kinetic energy.

3.3. Gravitational waves

We here recall the results of Damour & Esposito-Farèse (1992) and Wagoner & Kalligas(1997), concerning the interaction of a scalar wave with interferometric detectors. Far from any source of gravitational radiation and in a weak field, the metric writes:

$$\tilde{g}_{\mu\nu} = a^2(\varphi_0)\left(\eta_{\mu\nu} + \frac{1}{R}\left[h^*_{\mu\nu} + 2\alpha_0 F\eta_{\mu\nu}\right] + O(1/R^2)\right); \tag{18}$$

where $\eta_{\mu\nu}$ is the flat (Minkowskian) metric, $h^*_{\mu\nu}(t - R/c)$ and $F(t - R/c)$ are the $1/R$ components of the Einstein metric $g^*_{\mu\nu}$ and of the scalar field φ. The Riemann tensor of the physical metric can be written (at the first order) as the sum of two terms:

$$\tilde{R}^{(2)}_{0i0j} = -\frac{a^2(\varphi_0)}{2Rc^2}\frac{\partial^2 h^{*TT}_{ij}}{\partial t^2},$$

which is the spin-2 contribution to the wave (TT denotes the *transverse-traceless* part) and

$$\tilde{R}^{(0)}_{0i0j} = \frac{\alpha_0 a^2(\varphi_0)}{Rc^2}\left(\delta_{ij}\frac{\partial^2 F}{\partial t^2} - \frac{\partial^2 F}{\partial x^i \partial x^j}\right).$$

It is thus clear that monopolar waves interact with the detectors as well as quadrupolar ones. It is known that if one writes the geodesic equations in the transverse-traceless gauge, one sees that test masses have no *coordinate* change when a quadrupolar gravitational wave passes. But the photons measuring the distance between these two masses are affected by the wave. The opposite holds for monopolar waves: the photon travel is not affected (since they follow null geodesics, they cannot differentiate between Einstein and Fierz metric), but proof masses undergo coordinate change in the TT gauge as the wave passes.

The right quantity to compare with the quadrupolar wave amplitude at a distance d from the source $h_Q = h^{TT}_{ij}/d$ appears to be:

$$h_S(t) = \frac{2}{d}a^2(\varphi_0)\alpha_0 F(t), \tag{19}$$

where d is expressed in meters. This is the reason why we have plotted the function $F(t)$ in Figs. 11-13, as in Paper I. These three figures represent the three type of waveforms we have encountered. In (Fig. 11) the scalar field just "follows" the hydrodynamical evolution, having almost no effect on the hydrodynamical

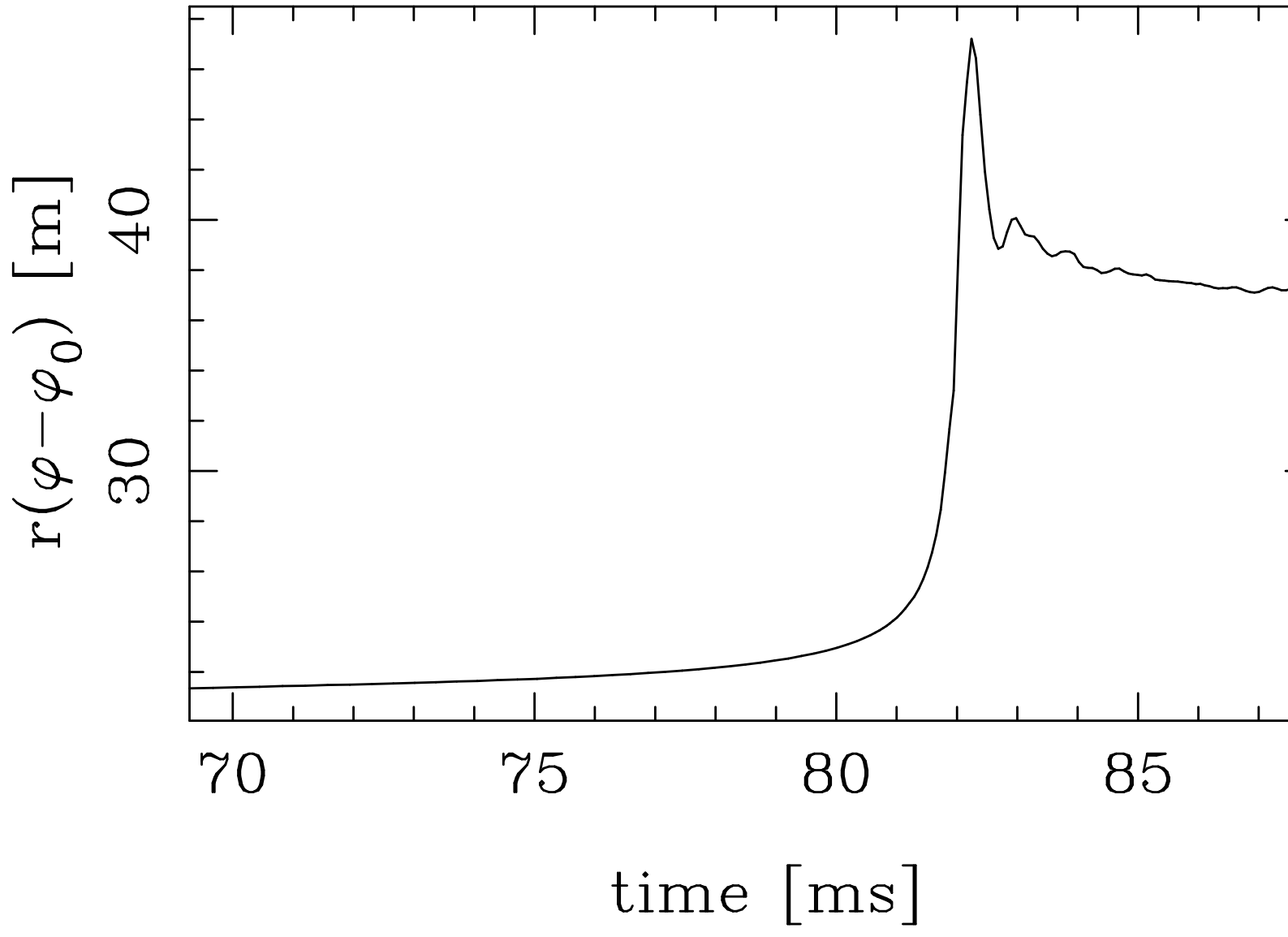

Fig. 11.— Resulting monopolar gravitational waveform (as a function of time), for the model C of Tab. 1

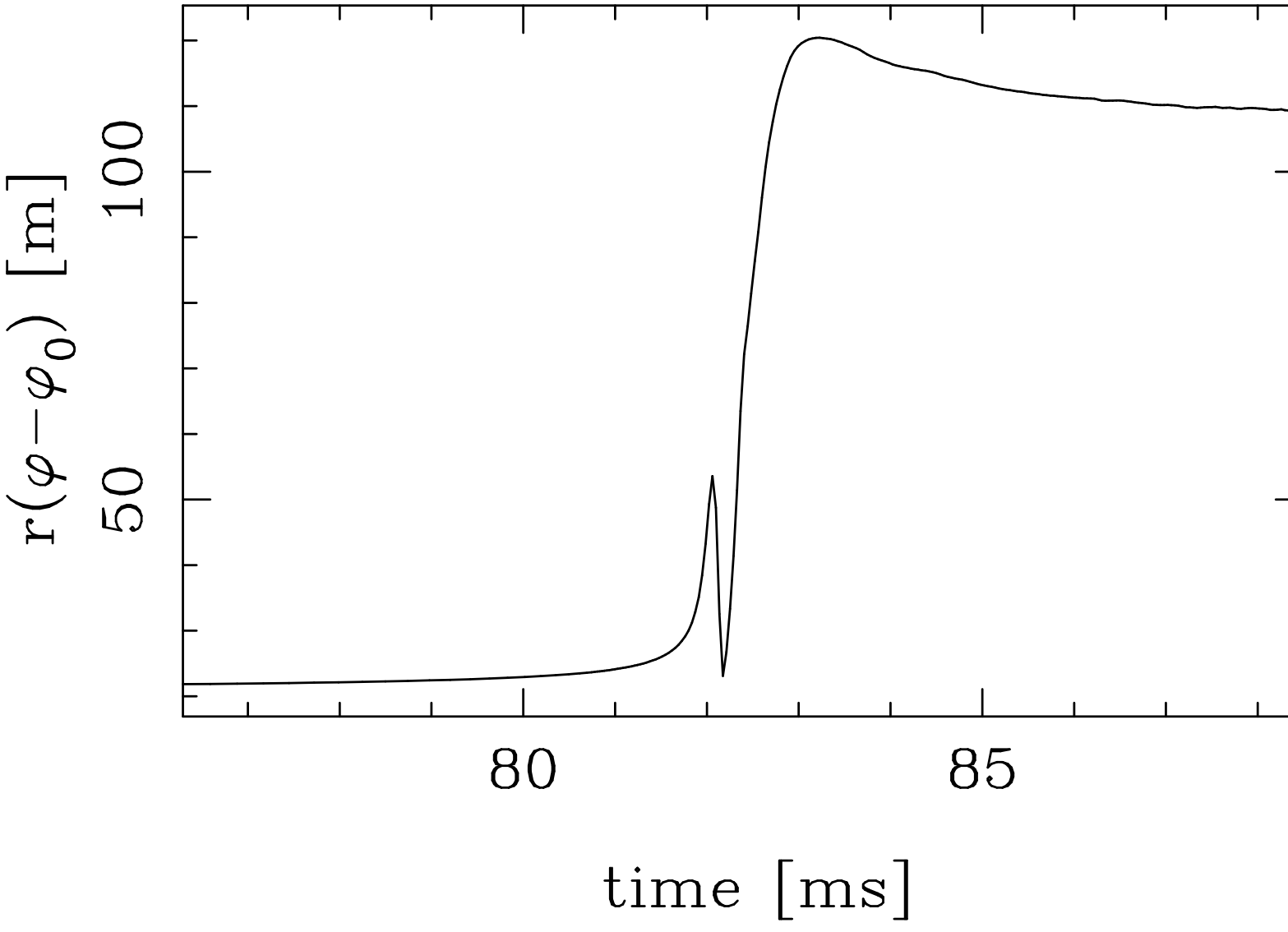

Fig. 12.— Resulting monopolar gravitational waveform (as a function of time), for the model D of Tab. 1

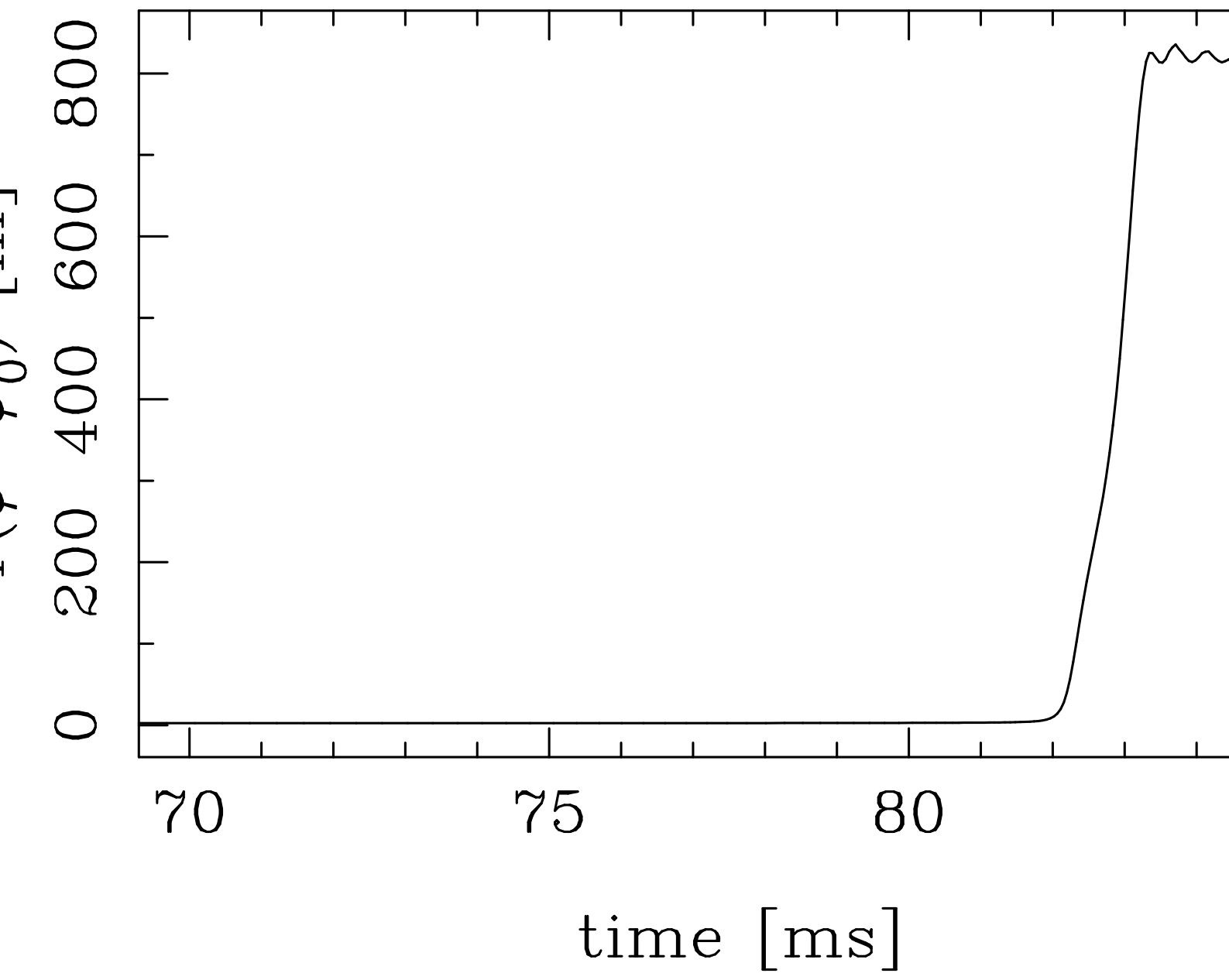

Fig. 13.— Resulting monopolar gravitational waveform (as a function of time), for the model E of Tab. 1

evolution. In (Fig. 12), it acts a little on this evolution and undergoes raise even after the bounce occurred. Finally, in (Fig. 13) the star undergoes a "spontaneous scalarization" and the waveform is very close to those shown in Novak (1998b). The parameters on which the waveform depends are essentially the β_0 (for the spontaneous scalarization to appear) and the final compactness of the star, which depends on the equation of state used (17). The more compact the star, the stronger the scalar field.

The results of Paper I, concerning the dependency of the amplitude on the scalar field parameter α_0 were retrieved: in the case of spontaneous scalarization the wave amplitude (19) goes as α_0, and as α_0^2 otherwise. Since this is the amplitude which interacts with the detectors and since it contains at least one factor α_0 (coming from the interaction of the wave and the detector, in weak field regime), which is strongly constrained by solar-system experiments (Williams et al.(1996) and Damour & Esposito-Farèse (1996)), the result may seem disappointing, if spontaneous scalarization is excluded (as suggest recent results from binary-pulsar timing, see Damour & Esposito-Farèse (1998)) and if one compares to the amount of released energy (Cf. 2. However, if we consider the case of the model D: taking $\alpha_0 = 3 \times 10^{-2}$, which is the maximal value compatible with the solar-system experiments, taking the detectability limit of VIRGO[3] (Caron et al.(1997)) 3×10^{-23} $\mathrm{Hz}^{-1/2}$ at 800 Hz (which is the characteristic frequency of our events), one sees that a collapse occurring closer than 10 kpc from us (half of our Galaxy) could be detected.

4. Conclusions

We have successfully studied the gravitational collapse leading to a neutron star, within the framework of a tensor-scalar theory, and this is the first study of a gravitational collapse, with the presence of shocks, in tensor-scalar gravity. We have shown that, if the parameters of the theory are such that the non-perturbative phenomenon involving the scalar field (the so-called "spontaneous scalarization") can be excluded, as seem to indicate results of Damour & Esposito-Farèse (1998), then the scalar field has a little influence on the hydrodynamical evolution of the collapse. If the case where spontaneous scalarization can occur, the run indeed indicated that the resulting neutron star had a very strong scalar charge and that it underwent strong characteristic oscillations. This gives us high confidence in our combined code. As far as gravitational waves are concerned, we have shown that, with α_0 and β_0 constrained with solar-system tests and binary-pulsar timing, such a collapse could be detected up to 10 kpc from us. From the opposite

[3]at the considered frequency, the sensitivity of LIGO is comparable

point of view, a non-detection of any monopolar wave, when a supernova occurs (when we have neutrino and/or electromagnetic signal), could give constraints on the parameter space of the tensor-scalar theory. The computed waveforms appear to be quite different from those of Paper I, meaning that, if monopolar waves from gravitational collapses could be detected, one could in principle differentiate between each type of collapse: Type II Supernova or collapsing neutron star. As a byproduct, we have developed and tested a new type of code, combining spectral methods and Godunov-type techniques. We hope to proceed to more complicated problems (in more than one dimension) in General Relativity (that is, without the scalar field), using, at each time step, HRSC methods for solving numerically the equations governing the evolution of matter (the Hydro-part) and spectral methods for solving numerically the equations governing the gravitational field equations (Einstein-part) just for the distribution of matter given at that time step by the Hydro-part. The experience gained in present work seems to be stimulating for such new strategy in Numerical Relativity.

We are indebted to Silvano Bonazzola for providing us with the "smooth" interpolation procedure, as well as for very useful discussions and reading of the manuscript. JN acknowledges financial support connected with a post-doctoral fellowship LAVOISIER from the French ministry of foreign affairs. This work has been partially supported by the Spanish DGES (grant number PB97-1432).

REFERENCES

Arnett, W. D., 1977, ApJ 218, p. 815

Bonazzola, S., 1998, private communication

Bonazzola, S., Gourgoulhon, E. and Marck, J. A., 1997, in: Relativistic Gravitation and Gravitational Radiation, Marck, J. A. and Lasota, J. P. (Eds.), Cambridge University Press, p. 257

Bonazzola, S. and Marck, J. A., 1991, J. Comp. Phys. 97, p. 535

Canal, R., 1990, in: Supernovae, Bludman, S. A., Mochkovitch, R. and Zinn-Justin, J. (Eds.), Les Houches, p. 155, North-Holland

Caron, B., Dominjon, A., Drezen, C. et al., 1997, in: Gravitational Waves: Sources and detectors, Ciufolini, I. and Fidecaro, F. (Eds.), p. 73, World Scientific Publishing

Damour, T. and Esposito-Farèse, G., 1992, Class. Quant. Grav. 9, p. 2093

Damour, T. and Esposito-Farèse, G., 1993, Phys. Rev. Lett. 70, p. 2220

Damour, T. and Esposito-Farèse, G., 1996, Phys. Rev. D 54, p. 1474

Damour, T. and Esposito-Farèse, G., 1998, Phys. Rev. D 58, 042001

Damour, T. and Polyakov, A., 1994, Nucl. Phys. B 423, p. 532

García-Bellido, J. and Quirós, M., 1990, Phys. Lett. B 243, p. 45

Gourgoulhon, E., 1991, A& A 252, p. 651

Harada, T., Chiba, T., Nakao, K. and Nakamura, T., 1997, Phys. Rev. D 55, p. 2024

Hawking, S. W., 1972, Comm. Math. Phys. 25, p.167

Ibañez, J. M., 1984, A& A 135, p. 382

Martí, J. M., 1997, in: Relativistic Gravitation and Gravitational Radiation, Marck, J. A. and Lasota, J. P. (Eds.), Cambridge University Press, p. 239

Müller, E., 1997, *Ibid* p. 273

Novak, J., 1998a, Phys. Rev. D 57, p. 4789

Novak, J., 1998b, Phys. Rev. D 58, 064019

Oppenheimer, J. R. and Snyder, H., 1939, Phys Rev. 56, p, 455

Romero, J., Ibañez, J. M., Martí, J. M. and Miralles, J. A., 1996, ApJ 462, p. 839

Salgado, M., Bonazzola, S., Gourgoulhon, E. and Haensel, P., 1994, A& A 291, p. 308

Scheel, M. A., Shapiro, S. L. and Teukolsky, S. A., 1995, Phys. Rev. D 51, p. 4208

Shapiro, S. L. and Teukolsky, S. A., 1983, in: Balck Holes, White Dwarfs and Neutron Stars, Wiley

Shibata, M., Nakao, K. and Nakamura, T., 1994, Phys. Rev. D 50, p. 7304

Van Riper, K. A., 1978, ApJ 221, p. 304

Wagoner, R. and Kalligas, D., 1997, in: Relativistic Gravitation and Gravitational Radiation, Marck, J. A. and Lasota, J. P. (Eds.), Cambridge University Press, p. 433

Williams, J. G., Newhall, X. X. and Dickey, J. O., 1996, Phys. Rev. D 53, p. 6730